American Mineralogist, Volume 92, pages 510–517, 2007

Experimental investigation of the breakdown of dolomite in rock cores at 100 MPa, 650–750 °C

Michael T. DeAngelis,[1] Theodore C. Labotka,[1,*] David R. Cole,[2] Mostafa Fayek,[1,2] and Lawrence M. Anovitz[1,2]

[1]Department of Earth and Planetary Sciences, University of Tennessee, Knoxville, Tennessee 37996-1410, U.S.A.
[2]Chemical Sciences Division, Oak Ridge National Laboratory, Oak Ridge, Tennessee 37831-6110, U.S.A.

Abstract

The kinetics of the breakdown reaction dolomite = periclase + calcite + CO_2 were investigated using cores of dolomitic marble. Two samples of Reed Dolomite from southwestern Nevada were cut into cylinders approximately 4 × 6 mm in size. The cores were sealed in gold capsules with isotopically enriched water ($H_2{}^{18}O$ or $HD^{18}O_{0.5}{}^{16}O_{0.5}$). The samples were heated in a cold-seal hydrothermal apparatus to 650–750 °C at 100 MPa for durations ranging from 2–59 days. The cores were then sectioned and examined by EPMA, XRD, and SIMS techniques. All experiments showed some amount of reaction regardless of duration or temperature. Reaction products occurred mainly along grain boundaries, fractures within grains, and along sample edges. Ion images and isotope-ratio analysis indicated that reaction products exchanged with infiltrating fluids. Reaction rates were calculated from measured extents of reaction, which were determined from automated EPMA modes. At 700 °C, we measured reaction rates ranging from 3.8×10^{-14} to 2.3×10^{-12} mol/mm^2·s. The extent of reaction is proportional to the square root of time, suggesting a diffusion-controlled process. A shrinking-core model for the dolomite breakdown reaction fits the grain-size data, suggesting that diffusion of H_2O and CO_2 through the mantle of reaction products controlled the rate. Apparent activation energies for that diffusion are ~283 ± 32 kJ/mol for coarse-grained samples and ~333 ± 36 kJ/mol for fine-grained samples. Initial reaction occurred relatively fast near the surface of dolomite grains, but continued diffusion through the reaction products ultimately controlled the rate of dolomite breakdown.

Keywords: Dolomite, kinetics, H_2O, CO_2

Introduction

Mineral assemblages in the crust commonly form as a result of reactions between rock and an infiltrating fluid; both reaction and infiltration are time dependent. Laboratory studies of reaction rates are generally performed with the use of mineral powders to approximate rock assemblages (e.g., Dachs and Metz 1988; Heinrich et al. 1986, 1989; Kase and Metz 1980; Kridelbaugh 1973; Lüttge and Metz 1991; Schramke et al. 1987; Tanner et al. 1985). Those studies were successful in describing mechanisms and rates of reactions, but the large porosities and surface areas of powders in direct contact with an abundant fluid phase differ considerably from low-permeability rocks (Lüttge and Metz 1993). To investigate kinetic processes under more realistic conditions, we conducted an experimental study that used dolomitic marble as starting material to determine the reaction textures and rates.

We investigated the breakdown of dolomite in H_2O-rich fluid. The dolomite–H_2O system is ideal to study the roles of grain-boundary transport and surface reaction in rocks experimentally. The system is relatively simple, having only four components with the reaction dolomite = calcite + periclase + CO_2. It is significant for the study of metamorphic fluid–rock interaction because the presence of periclase (or its retrograde equivalent brucite) is a hallmark of reaction between dolomite and H_2O-rich fluid (e.g., Kerrick 1970; Ferry 1991) and because the reaction generates porosity, which promotes fluid flow through the rock. Through use of samples of various grain size and texture, control of pressure and temperature conditions, and use of isotopically and chemically characterized fluids, we could determine the reaction textures, measure the rate, and model the rate-controlling process in the natural rock samples.

Methods

Experimental techniques

Two dolomitic marble samples were selected from the Reed Dolomite, Tonopah, Nevada (Fig. 1). The Reed Dolomite is a massive, brown to tan, medium- to coarse-grained dolomitic marble that contains rare thin layers of phyllite, quartzite, and calcitic marble (Richards et al. 1996). Sample LM (field sample number LM57), from Lone Mountain, Nevada, is light gray, homogeneous, and contains equant dolomite grains ranging in size from 0.25 to 0.50 mm in diameter. This sample is 95% dolomite, with minor amounts of quartz, and has a slightly friable texture. Sample MR (field sample number MR22-2), from Mineral Ridge, Nevada, is light gray to yellow in color. Average dolomite grain-size ranges from 0.5 to 1.0 mm in diameter, and the grains are irregular in shape. This sample also contains minor quartz veins and intergranular fractures.

The experimental design is similar to that of Lüttge and Metz (1993) in their study of dolomite + quartz stability. Small cores, approximately 4 mm in diameter and 5–7 mm in length, were drilled from each marble sample. The cores were placed within thin-walled, 5 mm gold tubes, approximately 7.5 cm in length. An aliquot of $H_2{}^{18}O$ or $HD^{18}O_{0.5}{}^{16}O_{0.5}$ was added to each sample, and the capsules were purged with CO_2 gas and welded closed. The water–dolomite [$CaMg(CO_3)_2$] molar

* E-mail: tlabotka@utk.edu

0003-004X/07/0004–510$05.00/DOI: 10.2138/am.2007.2164

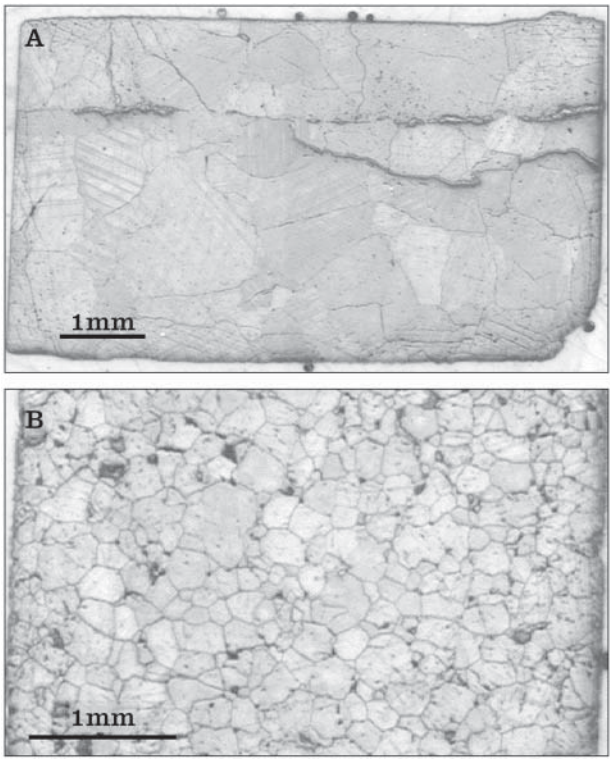

FIGURE 1. Thin sections of starting material. (**a**) Mineral Ridge dolomite sample MR22-2 with 0.5–1.0 mm average grain size. Note quartz vein in top half. (**b**) Lone Mountain dolomite sample LM57 with 0.25–0.5 mm average grain size.

ratio was approximately 5. The prepared capsules were placed in a vacuum oven for approximately 24 hours and then reweighed to ensure that there were no leaks. The capsule was placed in a cold-seal hydrothermal apparatus and pressurized and heated for the desired experiment duration. Each experiment was heated to the desired temperature over a period of 30 to 40 minutes, and the pressure was set to 100 MPa at the temperature. The experiment was isobarically quenched to ambient temperature over a period of 15 to 30 minutes. The capsule was then removed from the hydrothermal apparatus, weighed to test for leakage, placed in a vacuum line, frozen, and punctured. The CO_2 produced during reaction was separated cryogenically, and its yield was measured by manometry in a volume calibrated to ±1.0 μmol CO_2. The capsule was dried in a vacuum oven and reweighed to determine the amount of H_2O by difference. The core was removed, embedded in epoxy, and sectioned longitudinally.

Two series of experiments were performed. In the first, experiments were carried out at the constant T and P of 700 °C and 100 MPa, with durations ranging from 2 to 59 days. In the second, experiments were conducted at 100 MPa for 29 days, with temperatures ranging from 650 to 750 °C. All experiments were conducted in the stability field of calcite + periclase. Table 1 contains a detailed list of all experiments.

Analytical techniques

The extent of reaction was determined by electron microprobe (EPMA) analysis using a fully automated Cameca SX-50 at the University of Tennessee. Over 50 000 analyses were collected using the Oxford Instruments Energy Dispersive Spectrometer (EDS) FeatureScan option. Analyses were performed on a 10 μm grid across the entire sample. The mineral at each point was identified from the analysis, and the result was sorted into predefined mineral groups on the basis of X-ray counts (Taylor et al. 1996). Unclassified points generally made up less than 10% of the total and were found to be mixed-pixel points containing more than one mineral phase, commonly within reaction zones. A ±10% error is estimated for the extent of reaction on the basis of the mixed pixels. An unevaluated source of error is the irregular distribution of reacted areas in some experiments.

EPMA was also used to observe mineral-texture relationships by generating both back-scattered electron (BSE) and Ca, Mg, Si, and Fe X-ray images. The electron probe had an accelerating potential of 15 kV, a beam current of 4 nA, and a beam size of 1 μm. Images were generated by rastering over the area of interest, generally 256 × 256 μm, with a 2 μm step and a counting time of 10 ms per step. Stage scanning was used for most images, though beam scanning was used for detailed images smaller than 128 × 128 μm.

Quantitative mineral analyses were also collected with the EMP (Table 2). For these analyses, the EMP had an accelerating potential of 15 kV, a beam current of 6 nA, a beam size of 1 μm, and a counting time of 40 s for most elements. Natural samples of calcite, dolomite, and periclase were used as standards.

A Siemens D500 θ–θ powder X-ray diffractometer (XRD) was also used to identify minerals present in experimental samples. Analyses were obtained with the use of a Cu$K\alpha$ X-ray tube at 40 kV and 30 mA over an angular range of 5–50 °2θ with a 0.02° step and a 30 s counting time per step.

Ion images were obtained with the use of a Cameca 4f secondary ion mass spectrometer (SIMS) at Oak Ridge National Laboratory. Ion images were generated by rastering over a 250 × 250 μm area with a picoampere Cs^+ primary beam. A counting time of 30 s was used for ^{16}O images, and a counting time of 180 s was used for ^{18}O images.

RESULTS

Reaction products

All experiments, regardless of variation in time or temperature, showed some degree of reaction. The area of reaction generally is more extensive near the ends of the rock core than in the middle. Reaction products were located primarily along grain boundaries, fractures within grains, and along the outer edges of the rock core (Figs. 2a and 2b). Ion images of ^{18}O indicate that reaction products were isotopically enriched (Fig. 2c). In the MR samples, extensive reaction occurred along fractures and cleavage planes.

Despite grain-size differences between the starting materials, reaction textures are similar. The initial reaction texture along grain boundaries has a symmetrical appearance, with a narrow (<1 μm) center channel containing an Mg-rich phase surrounded on both sides by thicker (1–5 μm) bands of calcite (Fig. 3a). Periclase, brucite [$Mg(OH)_2$], and magnesite ($MgCO_3$) were all located within these narrow channels. The release of CO_2 during reaction resulted in an overall reduction in the volume of the solid-rock core and in an expansion of existing void space near the sites of reaction. Voids can be found between the calcite bands and the preexisting dolomite grains. As reaction continued, some dolomite grains were completely consumed; those reaction zones have a more mottled appearance (Fig. 3b). Complete consumption of some dolomite grains, however, only occurred in the two experiments at 750 °C. A few of the Mineral Ridge cores contain quartz veins. In those samples, dolomite reacted with the quartz to form forsterite and diopside.

All the experiments were conducted within the stability field of periclase. Periclase was generally too small to identify optically, although its presence was detected by XRD analysis. In the highest-temperature experiments, a few, very small (2–3 μm) nodules of periclase were identified by electron-probe analysis. Long blades (10–20 μm) of brucite formed in large void spaces between dolomite grains in one experiment, MR1 (Fig. 3c). Otherwise, brucite was not detected either in electron-probe or XRD.

Reaction products also crystallized on the outside of the dolomite rock cores. Calcite was sometimes observed as nodules attached to the outside of the cores, but usually only on the ends where the core was not in contact with the gold capsule

TABLE 1. Experimental data

Experiment	Starting material	Starting fluid composition	Temperature (°C)	Time (d)	CO_2 yield* (mol)	Final X_{CO_2}	Fluid weight		Core weight	
							Before (g)	After† (g)	Before (g)	After (g)
MR1	MR22-2	$HD^{18}O_{0.5}{}^{16}O_{0.5}$	650	46	–	–	0.04980	–	0.21897	0.21734
MR2	MR22-2	$HD^{18}O_{0.5}{}^{16}O_{0.5}$	700	2	–	–	0.03739	–	0.25635	0.25181
MR6	MR22-2	$HD^{18}O_{0.5}{}^{16}O_{0.5}$	700	29	1.83×10^{-4}	0.08	0.03805	0.03803	0.23775	0.22972
LM7	LM57	$HD^{18}O_{0.5}{}^{16}O_{0.5}$	700	29	4.56×10^{-5}	0.02	0.03829	0.03317	0.23297	0.23608
MR8	MR22-2	$H_2{}^{18}O$	700	14	4.43×10^{-5}	0.02	0.05252	0.04945	0.20438	0.2055
LM9	LM57	$H_2{}^{18}O$	700	59	1.19×10^{-4}	0.05	0.04517	0.03965	0.15257	0.15286
MR10	MR22-2	$H_2{}^{18}O$	700	59	3.49×10^{-4}	0.08	0.07011	0.06829	0.24581	0.23228
LM11	LM57	$H_2{}^{18}O$	700	43	6.90×10^{-5}	0.02	0.05308	0.05910	0.32147	0.31242
MR12	MR22-2	$H_2{}^{18}O$	700	43	2.61×10^{-4}	0.08	0.05168	0.05145	0.24101	0.22975
LM13	LM57	$H_2{}^{18}O$	700	14	1.07×10^{-4}	0.04	0.05722	0.04781	0.28564	0.29036
LM15	LM57	$H_2{}^{18}O$	700	2	3.79×10^{-5}	0.01	0.05730	0.05016	0.30933	0.3148
MR16	MR22-2	$H_2{}^{18}O$	650	29	8.28×10^{-5}	0.03	0.05652	0.05475	0.26393	0.26206
LM17	LM57	$H_2{}^{18}O$	750	33	–	–	0.05692	–	0.30273	0.28321
MR18	MR22-2	$H_2{}^{18}O$	750	29	8.32×10^{-4}	0.23	0.05610	0.04924	0.22431	0.19456
LM19	LM57	$H_2{}^{18}O$	650	29	3.45×10^{-5}	0.01	0.05642	0.05523	0.27804	0.27771

* MR1 AND MR2 CO_2 not measured; LM17 capsule burst after experiment and CO_2 was lost.
† Fluid weight after calculated by weight difference.

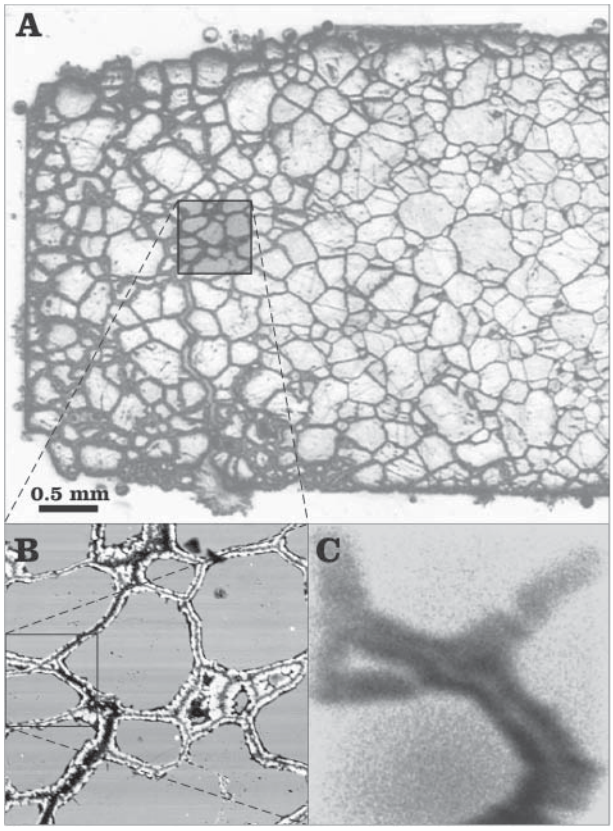

FIGURE 2. (**a**) Thin section photomicrograph of experiment LM7 (700 °C, 29 days). Areas of reaction are found primarily along grain boundaries, fractures within grains, and the outer edge of the sample. (**b**) LM7 BSE image showing distribution of reaction products along grain boundaries. (**c**) LM7 ^{18}O ion image showing an ^{18}O enrichment (white areas) in reaction products. Reaction products exchanged with infiltrating isotopically enriched fluid during crystallization.

during the experiment. Splays of nesquehonite ($MgCO_3{\cdot}3H_2O$), identified by X-ray powder diffraction, commonly crystallized between the outside of the rock core and the gold capsule during quench (Fig. 3d).

TABLE 2. Selected electron microprobe analyses of carbonate minerals

	MR dolomite	LM dolomite	MR calcite	LM calcite
$Mg(CO_3)$	45.1	44.5	8.57	9.13
$Ca(CO_3)$	55.0	54.7	90.9	90.8
$Fe(CO_3)$	0.15	0.73	0	0.14
Total	100.3	99.9	99.5	100.1
Cation basis	6	6	3	3
Mg	0.99	0.98	0.10	0.11
Ca	1.01	1.01	0.90	0.89
Fe	0	0.01	0	0
Total	2	2	1	1

Although most dolomite cores after experiment had an expected overall weight loss resulting from the release of CO_2 during reaction, a few had slight weight gains because of the presence of nesquehonite on the walls of some dolomite cores.

Extent of reaction with time

We considered that if the reaction were simply dolomite = calcite + periclase + CO_2, we would be able to use the CO_2 yield as a measure of the fractional extent of reaction, F. It was clear, though, from the presence of nesquehonite that some CO_2 and H_2O were combined with MgO on quench. We also found evidence for the presence of magnesite and brucite in some samples, which may also have formed during quench. We concluded that the amount of CO_2 was not a good measure of F. The more reliable measure of F is the amount of dolomite remaining after experimentation, which was determined by EPMA analysis. The textures and X-ray micrographs indicate that no dolomite formed during quench. The values of F are given in Table 3.

The average reaction rate, $\langle\overline{v}\rangle$, is given by the reaction extent divided by the time of the experiment. We normalized the rate to the total surface area with the assumption of spherical dolomite grains of equal size for each rock type, with diameters of 0.25 mm for LM and 0.50 mm for MR rocks; the areas are 7.7×10^5 and 3.9×10^5 mm^2/mol, respectively. For the time-series experiments, we found a range of average reaction rates from 3.8×10^{-14} to 2.3×10^{-12} $mol/mm^2{\cdot}s$ (Fig. 4). The rate of reaction is fast in the short-duration experiments for both the LM and MR samples. With longer experiment durations, rates were slower and nearly constant. The average rates for the MR samples were consistently greater than those for the LM samples; evidently

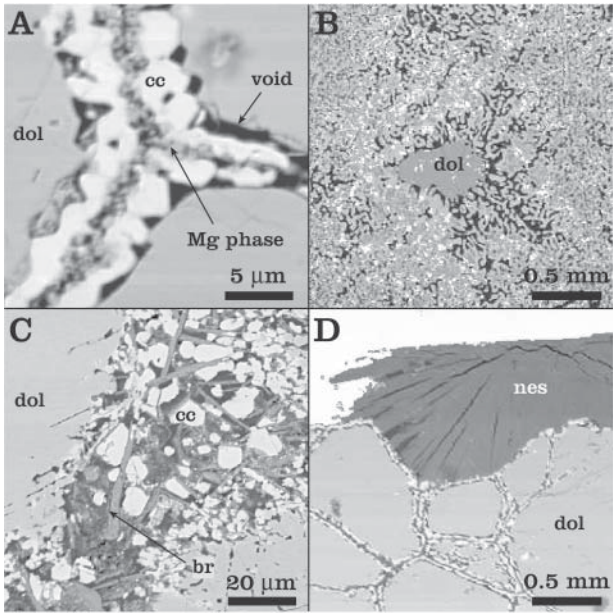

FIGURE 3. BSE images of reaction textures found in experimental samples. (**a**) Common grain boundary reaction textures from the LM9 (700 °C, 59 days) experiment show symmetrical bands of calcite split by narrow zone containing a Mg-rich phase. (**b**) Continued reaction in the MR18 (750 °C, 29 days) experiment shows complete consumption of most dolomite and resulting mottled reaction texture. (**c**) Long blades of brucite formed in the MR1 (650 °C, 46 days) experiment. (**d**) Splays of nesquehonite in the LM7 (700 °C, 29 days) experiment that formed between the rock core and the gold capsule wall.

TABLE 3. Measured extent of reaction from two different methods

Experiment	Extent by EMP point count	Extent by measured CO_2 yield*
MR2	15.4%	–
MR6	19.0%	3.5%
LM7	15.6%	14.5%
MR8	10.5%	4.0%
LM9	43.4%	14.4%
MR10	37.2%	26.2%
MR12	41.2%	20.0%
LM13	24.8%	6.9%
LM15	22.0%	2.3%
MR16	13.3%	5.8%
LM17	51.2%	–
MR18	62.8%	68.4%
LM19	7.4%	2.3%

* MR1 and MR2 CO_2 not measured; LM17 capsule burst after experiment and CO_2 was lost.

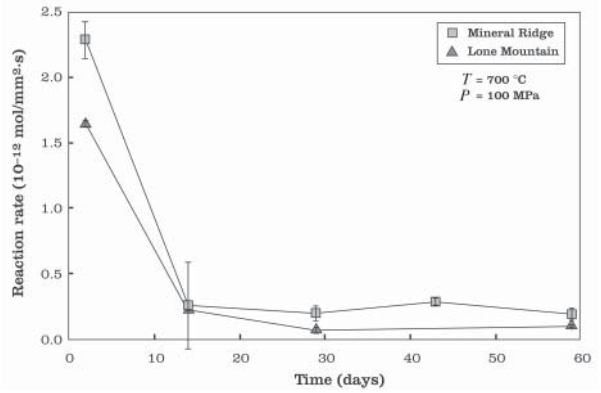

FIGURE 4. Reaction rate vs. the duration for each LM and MR time-series experiment.

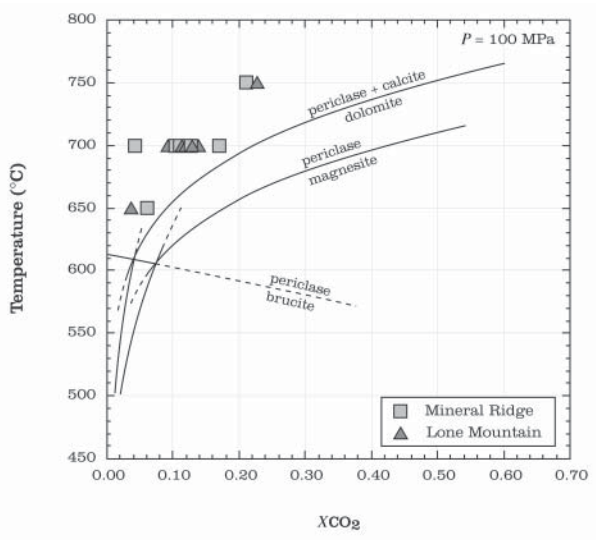

FIGURE 5. Final X_{CO_2} values for each experiment. The values were calculated from the fractional extent of reaction, F, determined by EPMA. CO_2 yields differed from the calculated values because of the formation of quench phases. The conditions of all experiments remained within the stability field of periclase + calcite (Holland and Powell 1990).

sample texture at least partly affected the reaction rate.

The change in fluid composition during the experiment may also have affected the rate. During reaction, the released CO_2 drove the fluid composition toward the equilibrium value (Fig. 5). The value of X_{CO_2} increased during reaction, thereby reducing the affinity (or Gibbs free energy of reaction, ΔG_r) and slowing the reaction. The T–X_{CO_2} conditions of all experiments, however, remained within the stability field of periclase + calcite.

The change in extent of reaction with time can indicate the overall control of the rate. Kinetic models of metamorphic reactions generally fall within three broad categories: heat-flow controlled, surface controlled, or diffusion controlled (Fisher 1978; Walther and Wood 1984; Rubie and Thompson 1985; Lasaga 1986, 1998; Ridley and Thompson 1986; Dachs and Metz 1988). Since all these experiments were conducted at constant temperature, changes in heat flow were not a consideration. Tanner et al. (1985) suggested that the model that best describes the experimental data could be determined by fitting an equation relating F to a function of time. A common approach to determine this relationship is to find a solution that best linearizes the F–t data (e.g., Kridelbaugh 1973; Tanner et al. 1985), yet there are numerous models for the rate (Brown et al. 1980). One that gives a decrease in rate with time is the Avrami–Erofe'ev model, $-\ln(1 - F)]^{1/n} = k(t - t_0)$, which seems to be valid for many nucleation and growth reactions in solids (Brown et al. 1980). The value of n gives the number of reac-

tion steps and dimensions in the nucleation and growth and is typically found to be 2–4. A power function fitted to our data by the non-linear Levenberg–Marquardt method gives a value of 0.5 for n with a χ^2 of 0.12 and an R of 0.71. Yet, a value for n of 0.5 is inconsistent with the Avrami model and suggests that a one-dimensional diffusion model in which F is proportional to the square-root of time is a better fit (Hulbert 1969; Brown et al. 1980; Rubie and Thompson 1985; Tanner et al. 1985). A power function fit gives $F(t) \propto \sqrt{t}$ with a $\chi^2 = 0.05$ and $R = 0.89$. The resulting fit, $F = 1.7 \times 10^{-4}\ t^{½}$, is shown in Figure 6. Although reaction textures indicate that reaction is initially surface-controlled at the dolomite grain surface, the rate-limiting process appears to have been diffusion through fractures, along grain boundaries, and through the products of reaction.

Extent of reaction with temperature

The extent of reaction at a given time depends on the temperature of reaction. Figure 7 shows $\langle\overline{v}\rangle$ for experiments conducted for 29 days at 750, 700, and 650 °C. The average rates range from a maximum of 7×10^{-13} at 750 °C to 3×10^{-14} mol/mm²·s at 650 °C. There is a clear separation on the basis of grain size with the coarser MR samples having a greater rate than the LM samples at the same temperature. The change in the logarithm of the rate with temperature, though, is similar for both samples.

The relation between $\ln\langle\overline{v}\rangle$ and $1/T$ in Figure 7 is linear, and it is tempting to interpret the slope as a measure of an activation energy of the reaction. However, the rate depends on the square root of time, and the values plotted in Figure 7 are not rate constants. Rather, if it is assumed that the reaction is a thermally activated process, then an apparent activation energy can be determined from the rate constants.

The rate constant, k, at 700 °C was found to be 2.89×10^{-8}/s (the square of the value in Fig. 6) for the combined experimental sample set. The rate model $F^2 = k \times t$ was applied to the data at all temperatures. The resulting values of $\ln(k)$ are plotted in Figure 8. All the data were fitted to a single line because the rate constants for MR are not consistently greater than those for LM. The result gives an apparent activation energy, E_a, of 324 ± 84 kJ/mol. This value is similar to other experimentally determined values for dehydration and decarbonation reactions (Tanner et al. 1985; Schramke et al. 1987; Heinrich et al. 1989). Tanner et al. (1985), for example, determined a value of E_a of 225 ± 78 kJ/mol for the decarbonation reaction calcite + quartz = wollastonite + CO_2. Wegner and Ernst (1983) determined a value of 757 kJ/mol for the dehydration of serpentine. The activation energy is at the low end of those for volume diffusion in solids but is within the range for reaction rates thought to be limited by diffusion (Lasaga 1981).

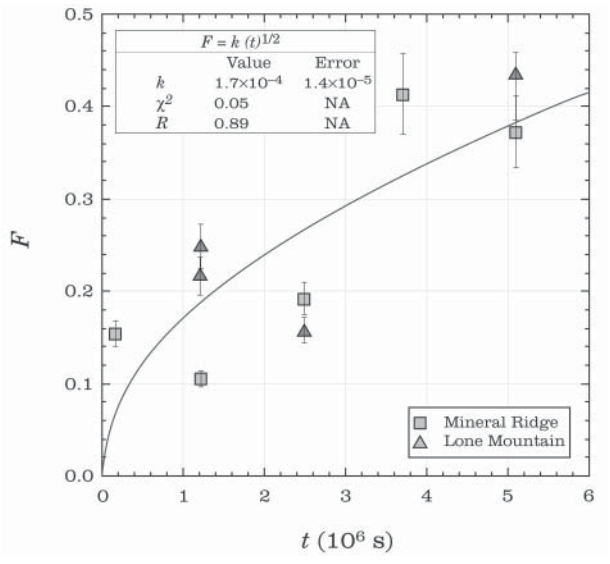

FIGURE 6. Plot of F vs. t at 700 °C. A nonlinear least-squares fit of a power function to the data shows that $F \propto \sqrt{t}$, suggesting that diffusion controlled the rate of the reaction.

DISCUSSION

Diffusion control

The values of F observed in our experiments are the result of several processes: transport of H_2O along grain boundaries to the dolomite surface, transport of CO_2 from the dolomite surface, reaction at the dolomite surface, and precipitation of the reaction products in the grain-boundary network. The rates we estimate include all those mechanisms, but the square-root dependence on time suggests that the rate-limiting step is diffusion. The reaction texture (Fig. 3) of a dolomite grain surrounded by reaction products suggests that the rate-limiting process could be the interdiffusion of CO_2 and H_2O through the reaction-product layer. With continued reaction, the core dolomite grain shrinks as a mantle of calcite and Mg-phases grows. Reaction progress can be thought of as a mass transfer of H_2O and CO_2 through the mantling layer. In nature, such a reaction can proceed as long as the temperature and mass-transfer coefficient (the ratio of mass

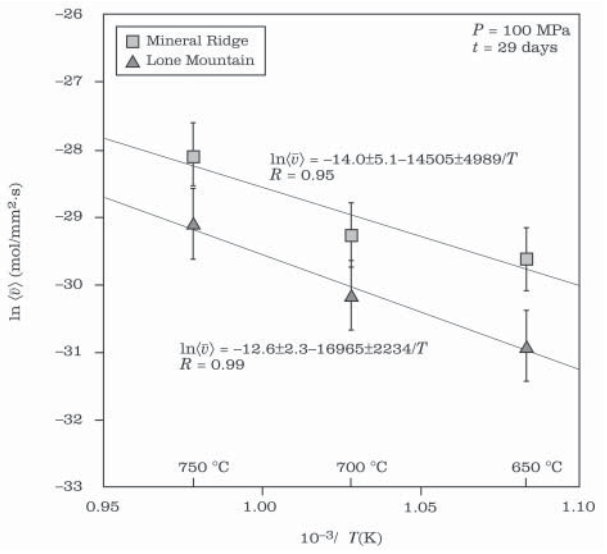

FIGURE 7. Average rate $\langle\overline{v}\rangle$ of the six experiments at different temperature. The errors are the standard error from an assumed 10% error in F. The rates show an Arrhenius-like relation with temperature. The apparent activation energy, though, is determined from the rate constants rather than from the average rates.

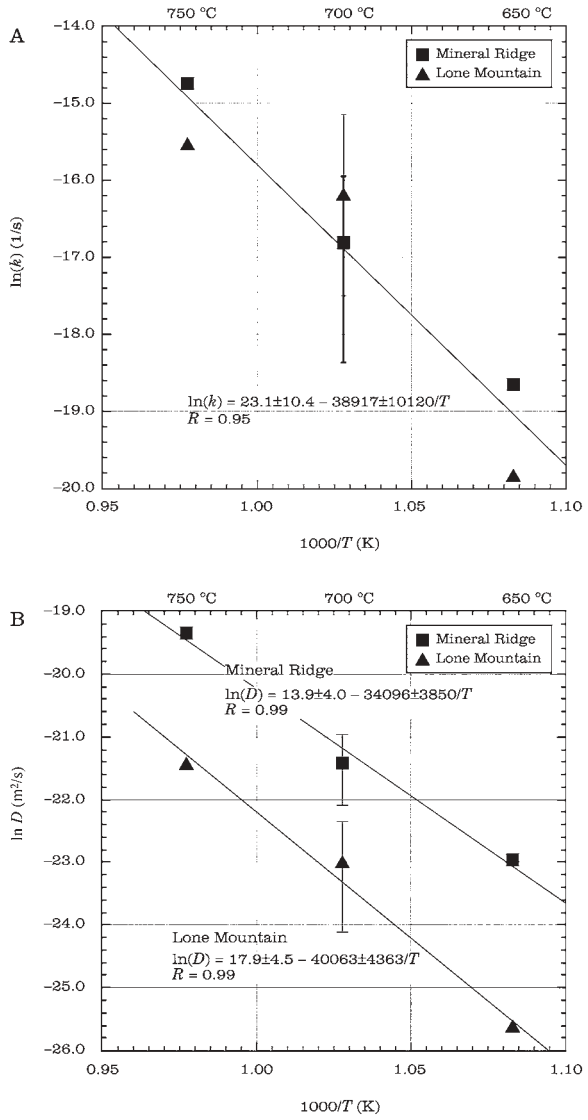

FIGURE 8. (**a**) Change in the rate constants from the reaction model $F = (k \times t)^{1/2}$ with temperature. An apparent activation energy of 324 ± 84 kJ/mol is given by the slope. (**b**) Apparent diffusion coefficients determined from the shrinking-core model of diffusion and reaction, giving apparent activation energies of 283 ± 32 and 333 ± 36 kJ/mol for the MR and LM samples, respectively. In both parts, the errors are given for the 700 °C experiments only, for which multiple experiments were done.

flux to concentration difference; Cussler 1997) allow transport through the layer.

The relation between diffusion and heterogeneous reaction has been described by Crank (1975), Cussler (1997), Glicksman (2000), and others. The process of dolomite breakdown can be described in terms of a shrinking core, where reactants and products diffuse through an alteration layer surrounding a reacting particle. The mass-transfer coefficient depends on the thickness of the alteration layer and is assumed to be $D/(r_0 - r)$, where D is the diffusion coefficient and r is the particle radius. The initial radius is r_0. Mass balance relates the radius with time as

$$r = r_0 - \left(\frac{2Dc_1}{c_2}t\right)^{1/2}$$

The coefficients c_1 and c_2 are the concentrations of H_2O at the outer and inner edges of the layer, respectively (Cussler 1997). The change in the radius with time gives the effective diffusion coefficient. The average grain radius in the 700 °C experiments was determined from the volume fraction remaining, $1 - F$. The result is shown in Figure 9. Least-squares fits to the lines are consistent with initial radii and have nearly identical slopes.

The value of D was determined from the linear fits of r to $\sqrt{t}$ with the assumption that the ratio c_1/c_2 is close to one (the equilibrium value of X_{H_2O} is ≈ 0.8). The diffusivity from the fits is ~1–8 × 10^{-10} mm^2/s and is similar to diffusivities in solids. The model was applied to the 650 and 750 °C experiments; the resulting values of ln(D) are shown in Figure 8b as a function of $1/T$; the slopes give apparent activation energies of ~283 ± 32 kJ/mol for MR samples and 333 ± 36 kJ/mol for LM samples. The apparent activation energy for the diffusion model is essentially the same as for the kinetic model (Fig. 8a) because both ln(D) and ln(k) are derived from the same parameter F.

A closure temperature can be calculated from the apparent activation energy and frequency factor for the diffusion model. Below that temperature, the interdiffusion of CO_2 and H_2O through the reacted layer is too slow to effect further reaction (Dodson 1973). The closure temperature, Figure 10, was calculated from the generalized equation given by Lasaga (1998) as a function of the cooling rate, s, and diffusion distance, a,

$$T_c = \frac{E/R}{\ln\left[2D_0RT_c^2/\left(a^2sE\right)\right]}$$

T_c is the closure temperature; E/R is the activation energy divided by the gas constant; and D_0 is the frequency factor. The range of temperature values results from the two values of the activation energy and frequency factor for the samples (Fig. 8b). As an example, the dolomite breakdown reaction in rocks with a grain radius of 0.1 mm would cease at 400–500 °C if the cooling rate were 1–1000 °C/m.y., a reasonable range of rates for regional and contact metamorphism. That temperature range, though, places the dolomite system in H_2O-rich fluids squarely in the brucite stability field.

Implications

Mineral powders are commonly used to determine reaction rates experimentally (Dachs and Metz 1988; Heinrich et al. 1986, 1989; Kase and Metz 1980; Kridelbaugh 1973; Lüttge and Metz 1991, 1993; Schramke et al. 1987; Tanner et al. 1985). Mineral powder reactants, though, have much greater surface areas than rocks do, resulting in fast reaction rates. The amount of time required for complete conversion of dolomite powders can be calculated using the reaction rates determined in this study. For example, if the powder experiment contained an amount of 50 µm diameter dolomite powder equivalent to the mass of a typical rock core (~250 mg), we would expect complete conversion of the dolomite powder in as little as 18 hours. This simple calculation, however, considers only differences in the surface area of reactants. If the larger permeabilities within mineral powder

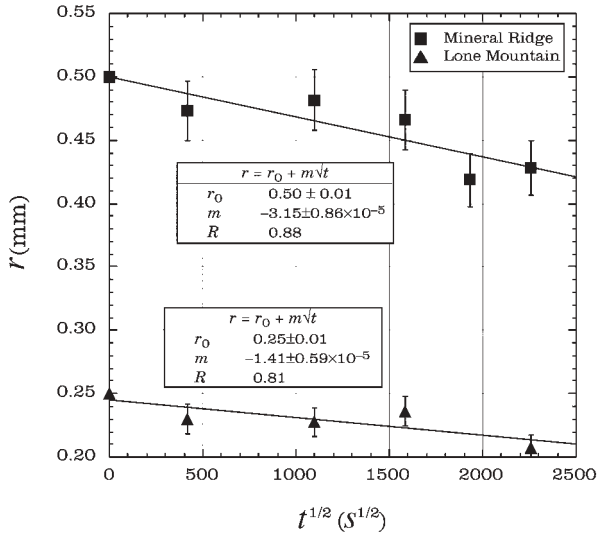

FIGURE 9. Radius of dolomite grains with time for the 700 °C experiments. The radii are calculated from the value of F with the assumption of radii r_0 of 0.5 and 0.25 mm for the MR and LM samples. The slopes are used to calculate an effective D from the shrinking-core model for diffusion and reaction. The errors are from the ± 10% error in determining F.

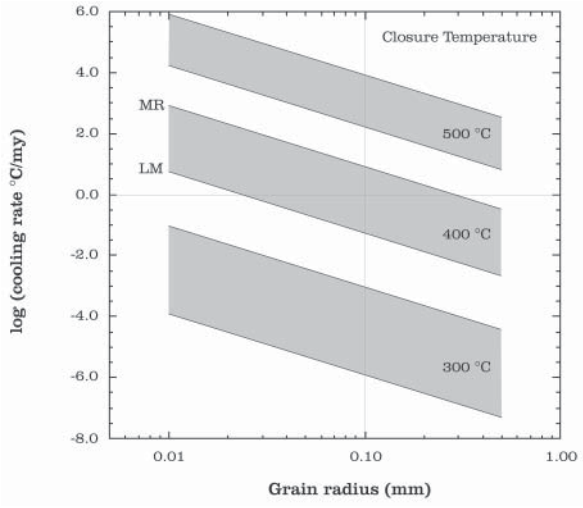

FIGURE 10. Closure temperature for the dolomite breakdown reaction, assuming that the reaction is limited by the rate of diffusion. The curves are calculated from the activation energies shown in Figure 8b. The top of each band represents the value for MR samples, and the bottom is the value for LM samples.

experiments were also included, faster rates of conversion should be expected since CO_2 residence times at sites of reaction would be diminished. Although Lüttge and Metz (1993) found little difference in the rate of the reaction dolomite + quartz = diopside + CO_2 between powder and rock-cylinder experiments, that reaction was locally interface-controlled rather than diffusion-controlled, as was the dolomite breakdown reaction studied here. Mineral-powder reactions should occur more rapidly, in general, than reactions that are controlled by transport.

An important difference between our experiments and many natural systems, though, is that our experimental system is closed. There is no continual resupply of H_2O near the site of reaction. This lack of continual movement of H_2O to the site of reaction and CO_2 away from it results in local X_{CO_2} increases that effectively reduce ΔG_r and slow reaction. These local increases in X_{CO_2} may explain the presence of magnesite in some of our reacted cores, even though our experimental temperatures are higher and the overall X_{CO_2} is lower than are required for the formation of magnesite.

The rock-core experiments were intended to better emulate metamorphic processes in the laboratory. However, they still lack several features of true geologic processes. While fluid flow in the crust is a combination of momentum transport and mass transport—infiltration and diffusion—our experiments cannot adequately address the interplay between reaction and infiltration; they were conducted isobarically and isothermally. Nevertheless, the experiments examined the interplay between grain-boundary diffusion and surface reaction in real rocks. In that regard, the experiments were successful and make it clear that texture and fracture density play significant roles in the overall reaction rate. Reaction rate was found to be faster in the coarser-grained and fractured MR samples than in the finer-grained LM samples. For both samples, however, the rate of dolomite breakdown seems to have been controlled by the diffusion of CO_2 and H_2O through the mantling products.

ACKNOWLEDGMENTS

This manuscript is a portion of M.T. DeAngelis's M.S. thesis work at the University of Tennessee, Knoxville. We sincerely appreciate the helpful comments and discussions with Linda C. Kah and Lawrence A. Taylor throughout the duration of this project. Many thanks also to Allan Patchen for help with EPMA analyses and to Bill Deane for help with XRD analyses. We sincerely thank Andreas Lüttge and an anonymous reviewer for their help in improving the manuscript. Funding for this work was provided by the National Science Foundation grant EAR-0087553 and the Division of Chemical Sciences, Geosciences, and Biosciences, Office of Basic Energy Sciences, U.S. Department of Energy. Oak Ridge National Laboratory is managed and operated by UT-Battelle for the U.S. Department of Energy under contract DE-AC05-00OR22725.

REFERENCES CITED

Brown, M.E., Dollimore, D., and Galwey, A.K., Eds. (1980) Reactions in the solid state, 22, 340 p. Comprehensive Chemical Kinetics, Elsevier, Amsterdam.
Crank, J. (1975) The mathematics of diffusion, 414 p. Clarendon Press, Oxford.
Cussler, E.L. (1997) Diffusion: Mass transfer in fluid systems, 580 p. Cambridge University Press, U.K.
Dachs, E. and Metz, P. (1988) The mechanism of the reaction 1 tremolite + 3 calcite + 2 quartz = 5 diopside + 3 CO_2 + 1 H_2O: results of powder experiments. Contributions to Mineralogy and Petrology, 100, 542–551.
Dodson, M.H. (1973) Closure temperature in cooling geochronological and petrological systems. Contributions to Mineralogy and Petrology, 40, 259–274.
Ferry, J.M. (1991) Dehydration and decarbonation reactions as a record of fluid infiltration. In D.M. Kerrick, Ed., Contact Metamorphism, 26, p. 351–391. Reviews in Mineralogy, Mineralogical Society of America, Chantilly, Virginia.
Fisher, G.W. (1978) Rate laws in metamorphism. Geochimica et Cosmochimica Acta, 42, 1035–1050.
Glicksman, M.E. (2000) Diffusion in solids, 472 p. Wiley, New York.
Heinrich, W., Metz, P., and Bayh, W. (1986) Experimental investigation of the mechanism of the reaction: 1 tremolite + 11 dolomite = 8 forsterite + 13 calcite + 9 CO_2 + 1 H_2O An SEM study. Contributions to Mineralogy and Petrology, 93, 215–221.
Heinrich, W., Metz, P., and Gottschalk, M. (1989) Experimental investigation of the kinetics of the reaction 1 tremolite + 11 dolomite = 8 forsterite + 13 calcite + 9 CO_2 + 1 H_2O. Contributions to Mineralogy and Petrology, 102, 163–173.
Holland, T.J.B. and Powell, R. (1990) An enlarged and updated internally consistent thermodynamic data set with uncertainties and correlations: the system K_2O–Na_2O–CaO–MgO–MnO–FeO–Fe_2O_3–Al_2O_3–TiO_2–SiO_2–C–H_2–O_2.

Journal of Metamorphic Geology, 8, 89–124.
Hulbert, S.F. (1969) Models for solid-state reactions in powdered compacts: a review. British Ceramic Society Journal, 6, 11–20.
Kase, H. and Metz, P. (1980) Experimental investigation of the metamorphism of siliceous dolomites: IV. Equilibrium data form the reaction: 1 diopside + 3 dolomite = 2 forsterite + 4 calcite + 2 CO_2. Contributions to Mineralogy and Petrology, 73, 151–159.
Kerrick, D.M. (1970) Contact metamorphism in some areas of the Sierra Nevada, California. Geological Society of America Bulletin, 81, 2913–2938.
Kridelbaugh, S.J. (1973) The kinetics of the reaction: calcite + quartz = wollastonite + carbon dioxide at elevated temperatures and pressures. American Journal of Science, 273, 757–777.
Lasaga, A.C. (1981) Rate laws of chemical reactions. In A.C. Lasaga and R.J. Kirkpatrick, Eds., Kinetics of Geochemical Processes, 8, p. 1–66. Reviews in Mineralogy, Mineralogical Society of America, Chantilly, Virginia.
——— (1986) Metamorphic reaction rate laws and development of isograds. Mineralogical Magazine, 50, 359–373.
——— (1998) Kinetic Theory in the Earth Sciences, 811 p. Princeton University Press, New Jersey.
Lüttge, A. and Metz, P. (1991) Mechanism and kinetics of the reaction 1 dolomite + 2 quartz = 1 diopside + 2 CO_2 investigated by powder experiments. Canadian Mineralogist, 29, 803–821.
——— (1993) Mechanism and kinetics of the reaction: 1 dolomite + 2 quartz = 1 diopside + 2 CO_2: a comparison of rock-sample and of powder experiments. Contributions to Mineralogy and Petrology, 115, 155–164.
Richards, I.J., Labotka, T.C., and Gregory, R.T. (1996) Contrasting stable isotope behavior between calcite and dolomite marbles, Lone Mountain, Nevada. Contributions to Mineralogy and Petrology, 123, 202–221.
Ridley, J. and Thompson, A.B. (1986) The role of mineral kinetics in the development of metamorphic microtextures. In J.V. Walther and B.J. Wood, Eds., Fluid-rock interactions during metamorphism, 5, p. 154–193. Advances in Physical Geochemistry, Springer, New York.
Rubie, D.C. and Thompson, A.B. (1985) Kinetics of metamorphic reactions at elevated temperatures and pressures: an appraisal of available experimental data. In A.B. Thompson and D.C. Rubie, Eds., Metamorphic reactions, kinetics, textures, and deformations, 4, p. 27–79. Advances in Physical Geochemistry, Springer, New York.
Schramke, J.A., Kerrick, D.M., and Lasaga, A.C. (1987) The reaction muscovite + quartz = andalusite + k-feldspar + water. Part 1. Growth kinetics and mechanism. American Journal of Science, 287, 517–559.
Tanner, S.B., Kerrick, D.M., and Lasaga, A.C. (1985) Experimental kinetic study of the reaction: calcite + quartz = wollastonite + carbon dioxide, from 1 to 3 kilobars and 500 to 850 °C. American Journal of Science, 285, 577–620.
Taylor, L.A., Patchen, A., Taylor, D.H., Chambers, J.G., and McKay, D.S. (1996) X-ray digital imaging and petrography of lunar mare soils: Data input for remote sensing calibrations. ICARUS, 124, 500–512.
Walther, J.V. and Wood, B.J. (1984) Rate and mechanism in prograde metamorphism. Contributions to Mineralogy and Petrology, 88, 246–259.
Wegner, W.W. and Ernst, W.G. (1983) Experimentally determined hydration and dehydration reacton rates in the system MgO–SiO_2–H_2O. American Journal of Science 283-A, 151–180.

Manuscript received November 22, 2005
Manuscript accepted October 14, 2006
Manuscript handled by Matthias Gottschalk